Journal of Biomechanical Science and Engineering

Vol. 4, No. 3, 2009

Novel Image Analysis for Trajectory of Microtubules Gliding on Kinesins with Tip Detection*

Shukei SUGITA**, ***, Naoya SAKAMOTO****, Toshiro OHASHI****, ***** and Masaaki SATO**, ****

**Department of Biomedical Engineering, Graduate School of Biomedical Engineering, Tohoku University,
6-6-01 Aramaki-aza-Aoba, Aoba, Sendai 980-8579, Japan
*** Present address: VCAD System Research Program, RIKEN,
2-1 Hirosawa, Wako 351-0198, Japan
E-mail: ssugita@riken.jp
****Department of Bioengineering and Robotics, Graduate School of Engineering, Tohoku University,
6-6-01 Aramaki-aza-Aoba, Aoba, Sendai 980-8579, Japan
*****Present address: Division of Human Mechanical Systems and Design, Graduate School of Engineering, Hokkaido University,
N13, W8, Kita, Sapporo 060-8628, Japan

Abstract

Control of the gliding directions of kinesin-driven microtubules (MTs) *in vitro* has good feasibility for the development of nano-scale transport systems. A requirement for the control of transporters in these systems includes detecting the positions of gliding MTs; however, no studies have reported on the monitoring of the positions of gliding MTs. Here, we suggest an algorithm to detect tip coordinates of gliding MTs by binarization, skeletonization, and filtration of fluorescent images of MTs. The algorithm was first applied to artificially drawn segments with given lengths (10–80 pixels), widths (1–10 pixels), and curvature radii (20–120 pixels) to verify the effect of the sizes of MTs on accuracy of tip coordinates extracted by the algorithm, and error was estimated by referring to the true coordinates. The estimated errors were as small as 2 pixels in the width and were not affected by the length and the curvature radius, indicating that our algorithm is useful to extract the tips of MTs. The algorithm was subsequently applied to images of gliding MTs. Since distances from the trajectories of the MTs to the centers of gravity of the MTs (3.7 ± 2.1 pixels) were significantly larger than those to the tips (1.9 ± 0.5 pixels), the use of the tips as representative points of gliding MTs was verified. A detection method using tips of MTs, as suggested in this study, may be a useful technique for monitoring each MT in nanoscale transport systems.

Key words: Image Analysis, Tip Detection, Microtubule, Kinesin, Nano-Scale Transport System

1. Introduction

Kinesins are nano-scale motors that move along cytoskeletal networks of microtubules (MTs) in cells to efficiently transport vesicles and protein complexes using the energy released from ATP hydrolysis [1, 2]. The gliding movements between kinesins and MTs have recently been suggested for the development of nano-scale transport systems that can transport nano-scale objects such as DNA [3] and antibodies [4] on a chip [5]. An inverted

*Received 1 July, 2009 (No. 09-0299)
[DOI: 10.1299/jbse.4.404]

gliding assay, in which filaments glide on a protein-coated surface of a chip, has often been used for reconstruction of kinesin-MT transport systems *in vitro* [6].

Key requirements for the development of the transport systems include both controlling the gliding directions of MTs and monitoring their positions. Since MTs move in random directions on a kinesin-coated surface, a number of studies have tried to control these gliding directions of MTs with chemical patterns of motor proteins [7], fabricated topographical guides [4, 8], or a combination of these two techniques [9–11]. These methods allow most MTs to be guided in pre-determined patterns on a surface. In order to control the gliding directions of individual MTs, several groups have applied electrical fields and demonstrated the ability to steer gliding MTs in desired directions [12, 13]. While the directions of the applied electric fields were manually determined in these studies, this technique could lead to the development of flexible and efficient transport systems that control the directions of each transporter independently if the positions of the MTs could be detected automatically. However, there are no reports on monitoring the positions and motion of gliding MTs. For the development of the transport system, in which gliding MTs are independently directed with external controls, such as electric fields, the detection of the position and the movement (i.e., trajectory) of each MT is required.

The center of gravity is generally used for the representative point of a moving object. However, for the case of gliding MTs *in vitro*, the shapes of the gliding MTs must be considered. MTs sometimes exhibit curved shapes due to changes in the gliding directions, which may cause their centers of gravity to be at a greater distance from their trajectories, especially for longer MTs with smaller curvature radii. When an MT is propelled by several kinesins in the direction of their long axis, it is assumed that the trajectory of the MT is determined by the position of the kinesin that has captured the leading tip of the MT, and the remaining part of the MT follows the trajectory of the tip (Fig. 1). In these situations, the leading tip of the gliding MT should be a better marker for representing the position of the MT; however, to our knowledge, no studies have evaluated the efficiency of tracking the tips of MTs gliding on kinesins.

In the present study, we developed an algorithm that extracts tips of MTs using a kernel on binarized fluorescent images and evaluated the efficiency of using the tips as representative points of the movements of the gliding MTs. We first apply the algorithm to sample segments drawn from given coordinates, and verify the tip extraction by comparing extracted coordinates to the given coordinates. We subsequently apply the algorithm to images of gliding MTs and the coordinates of the tips of the MTs are compared to the trajectories of the MTs.

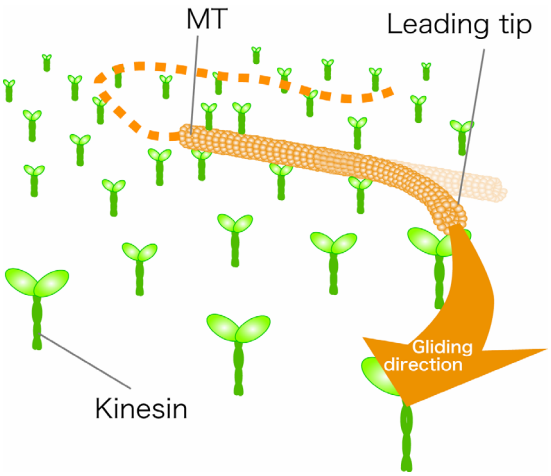

Fig. 1 A schematic of a gliding MT on a kinesin-coated surface. The gliding directions of the MT are assumed to be determined by the positions of kinesins capturing the MT.

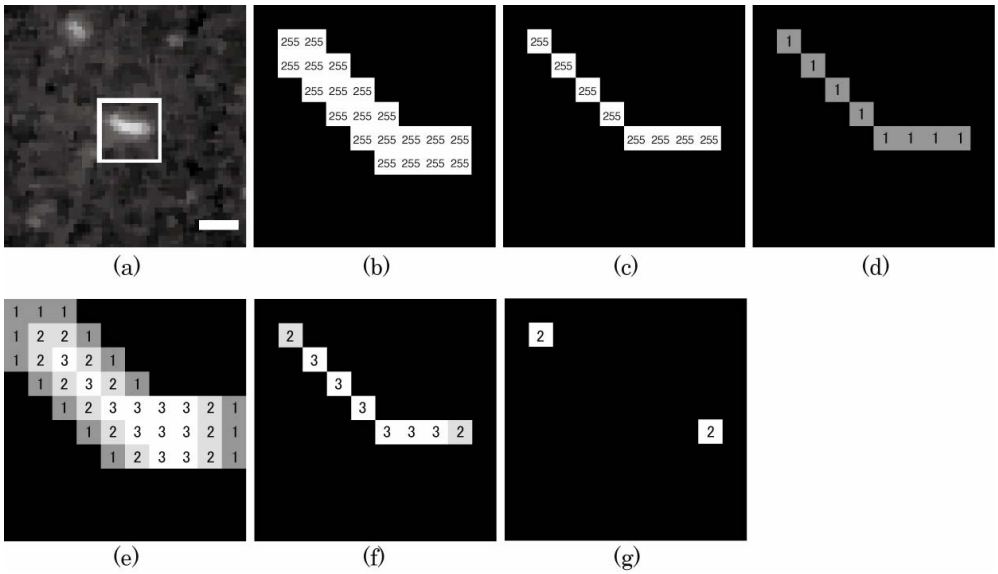

Fig. 2 Process for extracting tips of a single MT. Sample fluorescent image of the MT (a) was binarized (b), skeletonized (c), divided by 255 (d), and filtered with 3 × 3 kernel (e). Then, multiplication between the images (d) and (e) was performed (f), and finally, a binarizing process produced the extraction of the tips (g). The number in the illustrations shows the intensities in pixels; an intensity of 0 is omitted in these illustrations. Scale bar in (a) = 3 μm.

2. Analysis

2.1. Algorithm of image analysis

Analyses were conducted using an image analysis software (ImageJ, National Institutes of Health, Bethesda, MD, USA) on a personal computer (Intel Pentium 4, Microsoft Windows XP professional). Image processing was conducted by running a created macro in the software.

A schematic of the process to extract the tips of a line-shaped object in an image is shown in Fig. 2. This algorithm utilizes the property that only the end points of line-shaped objects have intensities of 2 after filtering with a kernel. An 8-bit grayscale image (Fig. 2(a)) was binarized with an appropriate threshold value by comparing with naked-eye detection of the MTs contours (Fig. 2(b)), and Zhang-Suen skeletonization [14] was performed to the image to generate an object 1 pixel wide (Fig. 2(c)). After the intensity of each pixel for the skeletonized image was divided by 255, in order to make pixels representing the line-shaped object have an intensity value of 1 and background a value of 0 (Fig. 2(d)), a filter with a 3 × 3 kernel with values of 1 for all was applied to the image (Fig. 2(e)). This process makes the resultant intensities of the end points 2. Then, multiplication was performed between the skeletonized image (Fig. 2(d)) and the filtered image (Fig. 2(e)), changing the intensities of all the pixels to 0 except the intensities those of the line-shaped object (Fig. 2(f)). Finally, the image was binarized with a threshold level of 2 to leave only the pixels whose intensities were 2. As a result, only the end points of the line-shaped object were extracted from the image (Fig. 2(g)).

2.2. Verification of image analysis

Coordinates of the tips extracted by the algorithm were compared to true coordinates of the tips of sample segments made from given coordinates to verify accuracy of the algorithm. First, we drew sample segments between given end points using the drawing tools of the image analysis software. The algorithm was applied to the image, and the tip coordinates extracted by the algorithm were compared to the given coordinates. The accuracy of the algorithm was evaluated by an error that was defined as the Euclidean distance between both the coordinates. Since MTs on fluorescent images exhibit a variety of

shapes (i.e., 3–5 pixels in width, more than 20 pixels in length, and more than 20 pixels in curvature radius (Fig. 5)) in our experimental setup (see 2.3), lengths (10, 20, 50, and 80 pixels), widths (1–10 pixels), and curvature radii (20, 40, 60, 80, 100, and 120 pixels) of sample segments were drawn to evaluate effects of object shape on estimated errors. Segments were also analyzed every 2° from 0–360°. The angle was defined by the horizontal line of the images and the line of the segment.

2.3. Image analysis of gliding microtubules

The images of gliding MTs were taken as previously reported [15]. Briefly, bovine tubulin containing 20% rhodamine-labeled tubulin were mixed and polymerized into MTs in BRB80 buffer (80 mM PIPES, 1 mM EGTA, 4 mM $MgSO_4$, pH 6.9) including 1 mM GTP at 37°C. We used the *Drosophila* kinesin with biotin carboxyl carrier protein at the C-terminal [16], which was kindly provided by Prof. H. Higuchi (University of Tokyo, Japan). To observe the gliding MTs *in vitro*, a flow cell fabricated with coverslips and spacers was sequentially filled with three kinds of protein solutions: 2 mg/ml biotinamidocaproyl labeled bovine serum albumin (biotinylated BSA), 2 mg/ml streptavidin solution, and 38 μg/ml of kinesin solution. The flow cell was then filled with 1 mM AMP-PNP solution containing MTs, followed by replacement with 1 mM ATP solution containing oxygen scavenger additives (1.5% β-mercaptoethanol, 1.5 mg/ml bovine serum albumin, 15 μM paclitaxel, 30 mM glucose, 120 μg/ml glucose oxidase, 30 μg/ml catalase) and 0.2% methylcellulose.

Time-lapsed images of the gliding MTs were captured with an inverted fluorescent microscope (IX-71, Olympus, Tokyo, Japan) equipped with a digital CCD camera (Cascade 512B, Nippon Roper, Tokyo, Japan). The rhodamine-labeled MTs were observed through a filter unit (U-MWIG, Olympus) and 60× oil immersion lens (NA = 1.45, Olympus, PLAPON 60XTIRFM). Images captured by the CCD camera were acquired using a personal computer every 1 s for 60 s, for a total of 61 slices of pixel images (512 × 512). The resolution of each image was 4 pixels/μm. The experiments were performed at room temperature of 20°C controlled by air conditioning.

Before applying the algorithm to the captured 8-bit grayscale images of MTs, the following image processing was conducted to produce well-contrasted images of smooth-shaped MTs: subtraction of background, enhancement of contrast, the application of a median filter, and binarization. This processing was first performed on the image at 0 s and the processed condition was then similarly applied to all the other images. The developed algorithm was then applied to the binarized images to extract the tips of the MTs. To evaluate the effect of changes in the threshold levels of the binarization on coordinates of the tips extracted by the algorithm, the images of smooth-shaped MTs were also binarized using higher and lower thresholds. The higher and lower thresholds were determined from levels that made the size of the MTs approximately 1 pixel bigger and 1 pixel smaller than the optimized size, respectively.

To compare the coordinates of the tips obtained in this study to general representative points of the positions of objects, coordinates of the centers of gravity of the MTs were also measured from the binarized images as stated above. Subsequently, the minimum distances from the coordinates of the tips and the centers of gravity to the trajectories of the MTs were calculated. The trajectories of the MTs were obtained from a total maximum projection image computed from time-lapsed images of the gliding MTs followed by a skeletonizing process. The mean of data for each MT was determined and is shown as mean ± standard deviation (SD). A Wilcoxon signed-ranks test was used to test for significant differences between the distances from the tips and the centers of gravity of MTs, with the level of significance at $p < 0.05$.

3. Results

3.1. Verification of algorithm

A typical image of a sample segment (5 pixels in width and 30 pixels in length), representative of the size of MTs on fluorescent images in our experiment, is shown in Fig. 3(a). By applying the algorithm to the image, the tips of the sample segment were extracted, as shown in Fig. 3(b). A merged image of the original segment and the extracted tips show that the extracted tips are located near the ends of the sample segment (Fig. 3(c)).

The effect of widths on errors for sample segments 30 pixels in length is shown in Fig. 4(a). There were no errors for sample segments 1 pixel in width, and the errors proportionally increased with an increase in width. The proportionality constant was 0.50, indicating that the errors were comparable to approximately half of the width of the sample segments. Since widths of MTs in fluorescent images ranged from 3 to 5 pixels in our experimental setup, the errors caused by the widths of the MTs on the images were estimated to be approximately 2 pixels. Effects of lengths and curvature radii of sample segments on errors are shown in Fig. 4(b) and (c), respectively. The errors did not change with any changes in the length and curvature radii of the segments. The effect of the angles of segments in images on errors is shown in Fig. 4(d). Although even small changes in angle affect the errors (approx. 2 pixels), these errors associated with changes in the angle were nearly constant. The changes in both the length and the curvature radius did not affect the errors, and although the widths of the segments did cause errors of only 2 pixels in the coordinates, we confirmed that the algorithm is applicable to extract the tip coordinates of MTs on fluorescent images.

3.2. Applying algorithm to images of gliding microtubules

Typical images of the tips of MTs, extracted using the algorithm, are shown in Fig. 5. As shown in Fig. 5(a)–(c), MTs polymerized *in vitro* have different lengths ranging from several pixels to approximately 50 pixels. Moreover, gliding MTs suddenly change their directions on the kinesin-coated surface and sometimes exhibit curved shapes. Curvature radii, calculated from arcs that passed through both end points of the MTs and had a least squares distance from points of the skeletonized MTs, were broadly distributed from 21 to more than 100 pixels (Fig. 5(d)–(f)). We assumed that the extracted coordinates of the tips of the MTs were not affected by the differences in MT length and curvature radii as indicated by the results of verifying the algorithm. In addition to the extracted tips of the MTs, the algorithm extracted midpoint of the MT shown in Fig. 5(f) because the shape of the MT after binarization exhibited a protrusion at the midpoint. In order to remove these undesirable points, the contours of the MTs should be smooth, and further improvements in image processing before application of the developed algorithms is required.

(a) (b) (c)

Fig. 3 Images of a sample segment and extracted tips. (a) A segment, 5 pixels in width and 30 pixels in length, generated from given coordinates. (b) Tips extracted by the algorithm from an image (a). (c) The sample segment merged with the tips obtained by subtracting image (a) from image (b).

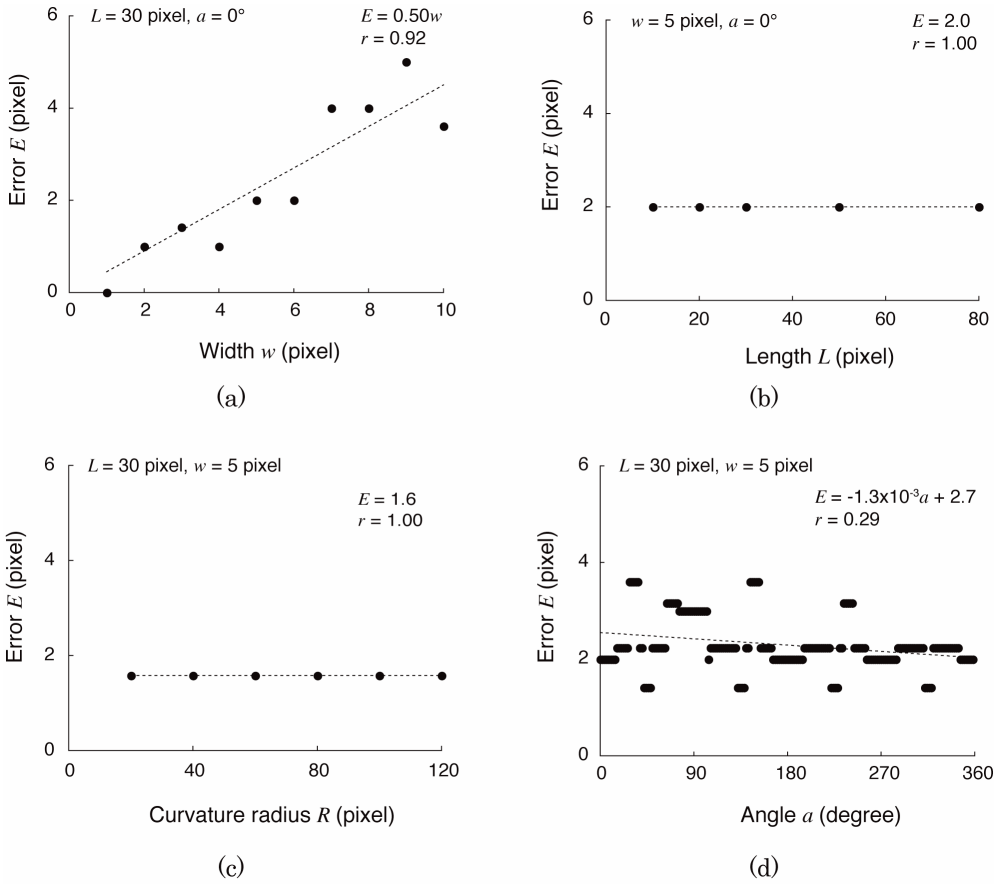

Fig. 4 Effects of (a) width, (b) length, (c) curvature radius, and (d) angle of sample segments on errors of coordinates of tips extracted by the algorithm. Dotted lines were obtained by least squares regression.

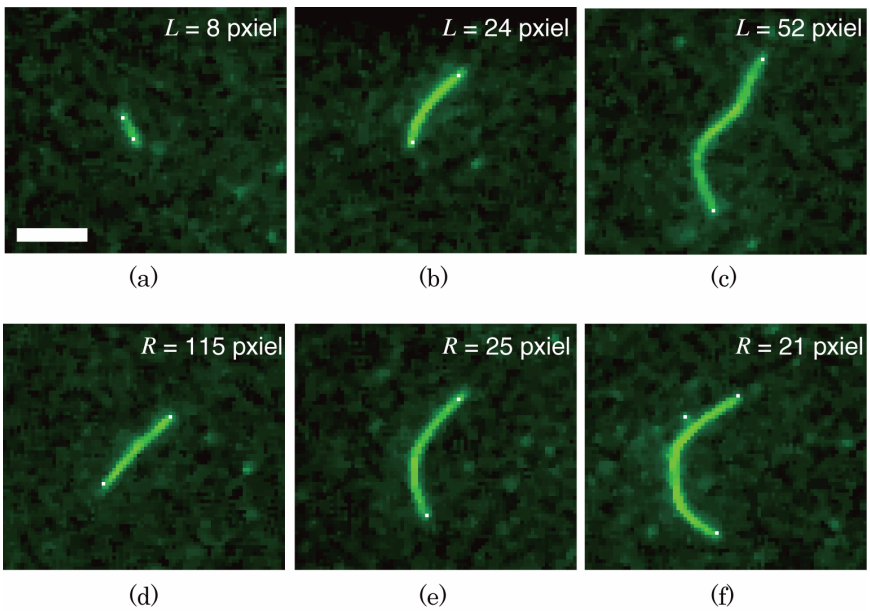

Fig. 5 Typical images of MTs (green) and extracted tips by the algorithm (white dots). Scale bar = 5μm. The MTs observed had a variety of lengths, such as L = (a) 8, (b) 24, and (c) 52 pixels, and curvature radii, such as R = (d) 115, (e) 25, and (f) 21 pixels.

Typical sequential images of the trajectory of a tip of a gliding MT is shown in Fig. 6(a). Although the trajectory of the MT obtained by superimposing the sequential images (Fig. 6(b)) was in good agreement with that of the tips extracted by the algorithm (Fig. 6(c)), a trajectory of the centers of gravity of the gliding MT merged with the Fig. 6(b) did not follow the trajectory of the gliding MT (Fig. 6(d)). The distances from the trajectories of the MTs to their tips were 1.9 ± 0.5 pixels (n = 10); significantly smaller than the distances from the trajectories of the MTs to their centers of gravity, 3.7 ± 2.1 pixels (n = 10) (Fig. 6(e)). The distances from the trajectories of the MTs to their centers of gravity were widely distributed from 1.4–7.3 pixels, whereas the distance to their tips was small (1.0–2.9 pixels). The larger distances to the centers of gravity were caused by the curved shape of the gliding MTs. In fact, there was a significant correlation between the distances to the centers of gravity and the angles, determined by dividing the lengths by the curvature radii (r = 0.746; p < 0.001; n = 487; data not shown). These results indicate that the distance to the centers of gravity increases for longer MTs exhibiting smaller curvature radii.

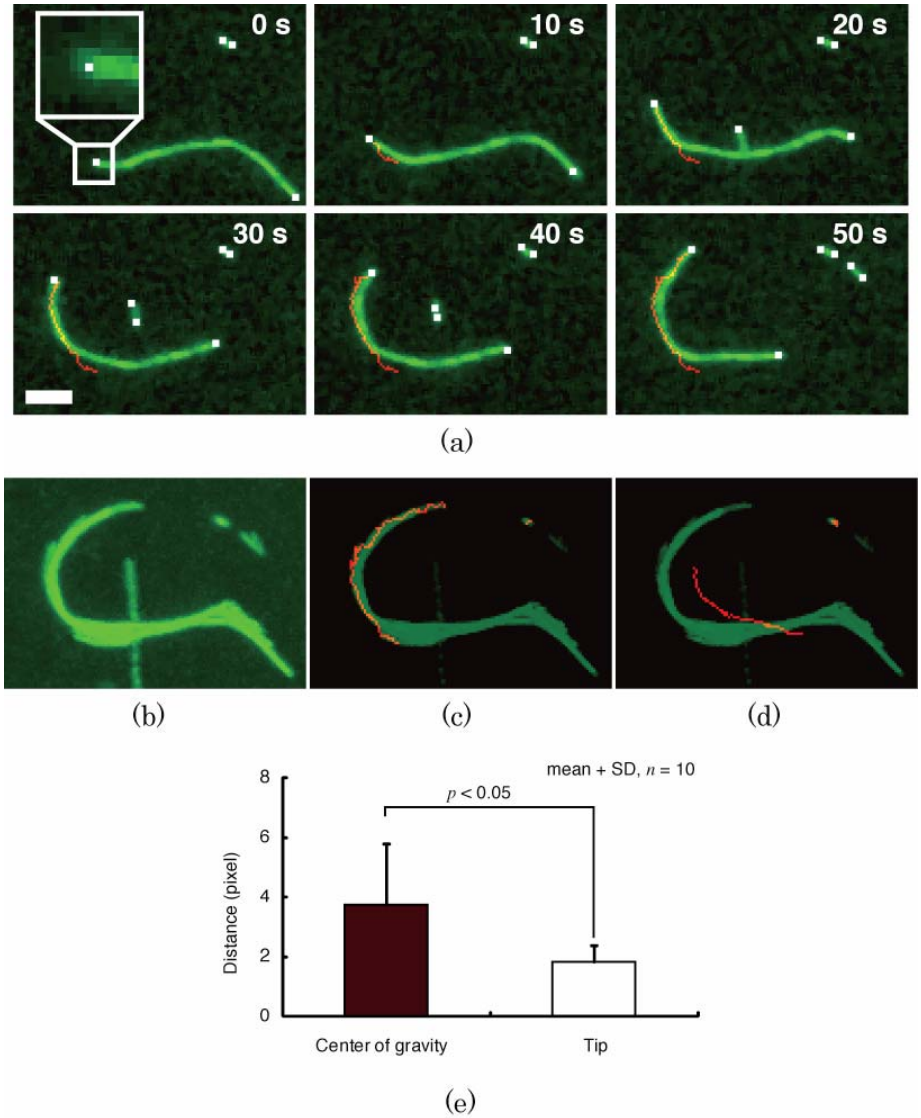

Fig. 6 Comparison between tips and centers of gravity of gliding MTs. (a) Time-lapsed images of the MTs gliding on a kinesin-coated surface merged with the images of end points (white dots) extracted by the algorithm and the trajectories of the tips (red lines). The end points extracted by the algorithm are enlarged to improve visibility, except in the inset image at 0 s. (b) Typical images of trajectories of gliding MTs. (c and d) Trajectories of (c) tips and (d) centers of gravity of the MTs (red lines) merged with (b). (e) Comparison of the minimum distances from tips and centers of gravity to trajectories of gliding MTs. Scale bar = 5 μm.

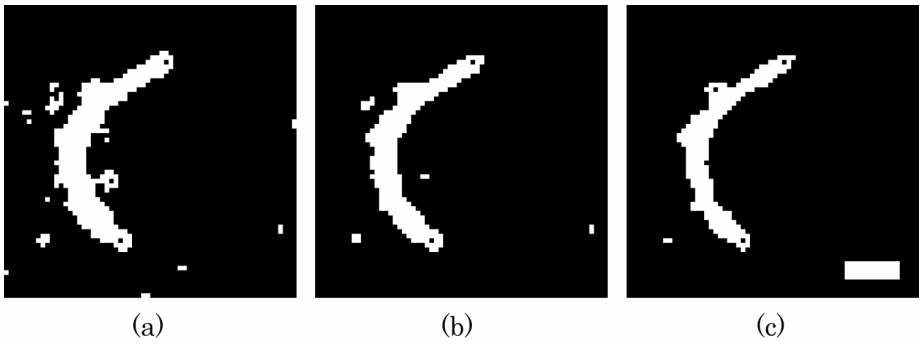

Fig. 7 Effect of threshold on changes in positions of tip coordinates (black dot in MT). The images were binarized by (a) low, (b) intermediate, (c) and high threshold levels. Scale bar = 3 μm.

The effect of thresholds for binarization on changes in the position of the tip coordinates of an MT extracted by the algorithm is shown in Fig. 7. Although the shape was bigger when the threshold level was lower, this did not affect the tip coordinates binarized with different threshold levels. The differences in tip coordinates at varying thresholds were 0.9 ± 0.9 pixels (low–intermediate, n = 155) and 1.1 ± 1.5 pixels (intermediate–high, n = 153).

4. Discussion

The center of gravity has generally been used as a representative position of an object. However, is the detection of the position of the center of gravity efficient as the representative position of the movement when a long and thinly-shaped object, such as an MT, produces a curvature radius by changing their gliding direction? The present study confirmed that the centers of gravity of MTs did not follow the trajectories of the gliding MTs, whereas their tips were in good agreement with these trajectories, as shown in Fig. 6. Therefore, the tips of MTs are important in representing the positions of gliding MTs.

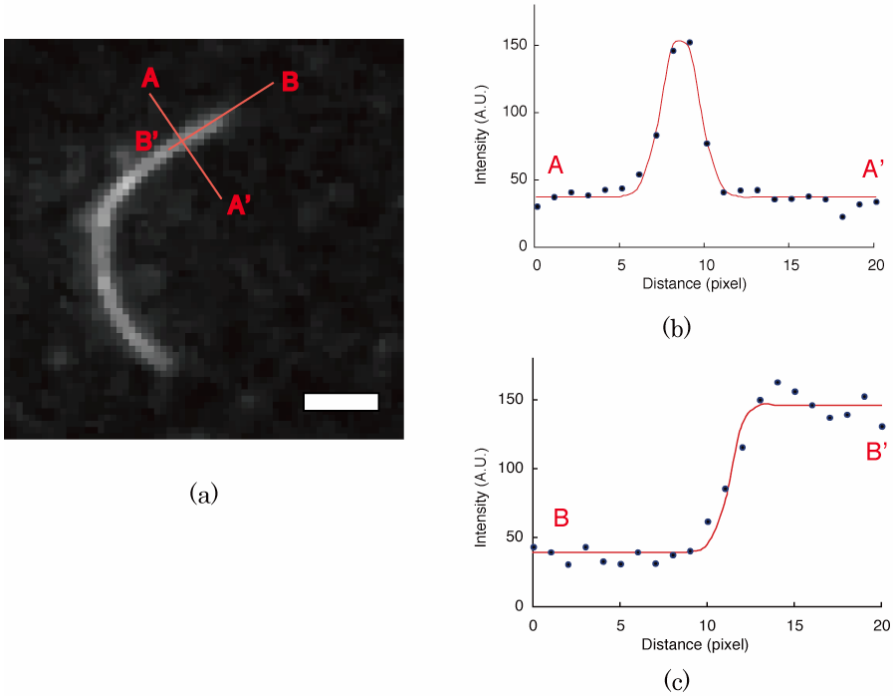

Fig. 8 Typical intensity profiles of an MT in long and short axis directions. From a fluorescent image of the MT (a), intensity profiles were measured in (b) short (A–A' in (a)) and (c) long (B–B' in (a)) axis directions. Scale bar = 3 μm. Curves fitted to (b) and (c) were determined as Gaussian and half Gaussian functions, respectively, by least squares regression.

Verification of the algorithm determined that lengths and curvature radii of sample segments did not affect errors, but increases in the width of sample segments increased the errors, and that the process of skeletonizing in the algorithm may have resulted in these errors. The skeletonizing process removes the intensities in pixels of objects from all edges until the objects have a width of 1 pixel. This process made the positions of the tips of the sample segments extracted by the algorithm located in long axis directions of the sample segments a half of the width, and was in a good agreement with the results suggesting that errors were expressed as $E = 0.50w$ in Fig. 4(a). However, the errors from the widths of the gliding MTs in fluorescent images were as small as 2 pixels in our experimental setup, and our algorithm was useful as a first step for automated extraction of the tips of MTs.

For the images of MTs, the tips of MTs extracted by the algorithm seemed to be located on the inside edges of the shapes of the MTs. Although a diameter of an MT is approximately 30 nm, the widths of the MTs observed in binarized images were measured as almost 1 μm, indicating that the width of the MTs has increased in the fluorescent images. Since the irradiation of light from a single point source causes an intensity distribution around the center of the source on an image, known as point-spread function, the spread in the width of MTs seemed to be caused by this distribution. This indicates that spreading should have occurred in long axis directions of the MTs as well; therefore, we analyzed fluorescent intensity profiles around the edges of an MT in both long and short axis directions, as shown in Fig. 8(a). For approximation of the intensity profiles, we used a Gaussian function that is often used for expressing the point-spread function [17], and results suggest that the intensity profiles can be well approximated with the Gaussian function and the half Gaussian function for the short (Fig. 8(b)) and long (Fig. 8(c)) axis directions, respectively. These results further indicate that the contours of the MTs in the fluorescent images spread in the long axis direction, and that the actual positions of tips of MTs are located inside rather than at the edge of binarized images of the MTs in the long axis direction. Although this may cause errors in estimates of the tip position, the errors would be on the order of 500 nm, thereby making the proposed algorithm effective for practical use.

Since the regulation of thresholds for binarization generally results in changes in the sizes of objects in grayscale images, we had first expected a displacement in tip coordinates of MTs when changing the threshold levels. However, differences in the tip coordinates were not observed for the three threshold levels tested (Fig. 7), and we believe that this resulted from the skeletonizing process. As shown in Fig. 8, the intensities gradually increase from the edges to the center of the MT indicating that the changes in the threshold levels cause the changes in the size of binarized MTs equivalently, in all directions. Since the size of the spreading object is decreased in all directions by the skeletonizing process, the tip coordinates extracted by the algorithm were not displaced from the changes in the threshold levels.

The skeletonizing process was conducted with the Zhang-Suen algorithm [14] which based on two subiterations. The first subiteration removes only the southeast boundary points and the northwest corner points, and the second subiteration removes northwest boundary points and the southeast corner points. Although this sequential two-step approach may generate errors 1 pixel by firstly removing the points of the one-side of objects, it is not considered to be large for practical use. In Fig. 4(d), errors caused by the changes in angles of segments were not cyclically changed with the period of 90° for some intervals of the angles (28–36°, 64–74°, 76–104°, 144–152°, 234–242°). In the angles, extracted tip coordinates was located 1 pixel horizontally or vertically distant from the periodically estimated coordinates. Therefore, differences of the errors from the periodical value are considered to be caused by the sequential two-step approach.

In this study, image analyses were conducted after all the time-lapsed images were

captured. However, real-time image analyses might be required in order to utilize the algorithm for the detection of the tips of MTs in the nano-scale transport systems. In the case that the algorithm was applied to a single image of kinesin-driven MTs with the size of 512 × 512 pixels and binarization was conducted automatically using pre-set threshold level, we confirmed that the tips of the MTs were extracted within 1 s. Since the gliding velocity of MTs *in vitro* were almost 1 μm/s at fastest[18], the algorithm in this study will be practically useful under systems capturing the images with microscopes.

In summary, we suggested an algorithm for the extraction of the tips of MTs from fluorescent images as markers of the positions of the gliding MTs. The algorithm was initially applied to drawn segments for verification of the algorithm, and results showed that changes in lengths and curvature radii of the segments did not affect errors in the tip extraction, but width of the segments affected the errors by nearly a half of their widths. However, the widths of MTs were approximately 3–5 pixels in the fluorescent images, so the errors of the tip extractions using the algorithm were considered to be negligible. By applying the algorithm to images of gliding MTs, tips of these MTs were successfully extracted. Unlike the centers of gravity, the tips of the MTs were in a good agreement with the trajectories of the gliding MTs. This algorithm may be useful for detecting the position of gliding MTs and assist in the development of controls for nano-scale transporters.

Acknowledgements

The authors thank Prof. Hideo Higuchi for technical support during preparation of the proteins. The authors acknowledge the support of the Tohoku University Global COE Program “Global Nano-Biomedical Engineering Education and Research Network Centre”.

References

(1) Sheetz, M.P., Vale, R., Schnapp, B., Schroer, T., and Reese, T., Vesicle movements and microtubule-based motors, *Journal Cell Science*, Vol. 5, (1986), pp. 181–188.

(2) Schroer, T.A., Schnapp, B.J., Reese, T.S., and Sheetz, M.P., The role of kinesin and other soluble factors in organelle movement along microtubules, *Journal of Cell Biology*, Vol. 107, No. 5 (1988), pp.1785–1792.

(3) Diez, S., Reuther, C., Dinu, C., Seidel, S., Mertig, M., Pompe, W., and Howard, J., Stretching and transporting DNA molecules using motor proteins, *Nano Letters*, Vol. 3, No. 9 (2003), pp. 1251–1254.

(4) Ramachandran, S., Ernst, K.H., Bachand, G.D., Vogel, V., and Hess, H., Selective loading of kinesin-powered molecular shuttles with protein cargo and its application to biosensing, *Small*, Vol. 2, No. 3 (2006), pp. 330–334.

(5) Hess, H., Matzke, C.M., Doot, R.K., Clemmens, J., Bachand, G.D., Bunker, B.C., and Vogel, V., Molecular shuttles operating undercover: A new photolithographic approach for the fabrication of structured surfaces supporting directed motility, *Nano Letters*, Vol. 3, No. 12 (2003), pp. 1651–1655.

(6) Howard, J., Hudspeth, A.J., and Vale, R.D., Movement of microtubules by single kinesin molecules, *Nature*, Vol. 342, No. 9 (1989), pp. 154–158.

(7) Suzuki, H., Yamada, A., Oiwa, K., Nakayama, H, and Mashiko, S., Control of actin moving trajectory by patterned poly (methylmethacrylate) tracks, *Biophysical Journal*, Vol. 72, No. 5 (1997), pp. 1997–2001.

(8) Riveline, D., Ott, A., Julicher, F., Winkelmann, D.A., Cardoso, O., Lacapère, J.J., Magnúsdóttir, S., Viovy, J.L., Gorre-Talini, L., Prost, J., Acting on actin: the electric motility assay. *European Biophysical Journal*, Vol. 27, No. 4 (1998), pp. 403–408.

(9) Hiratsuka, Y., T. Tada, K. Oiwa, T. Kanayama, and T.Q. Uyeda. Controlling the direction of kinesin-driven microtubule movements along microlithographic tracks, *Biophysical*

Journal, Vol. 81, No.3 (2001), pp. 1555–1561.

(10) Moorjani, S.G., Jia, L., Jackson, T.N., and Hancock, W.O., Lithographically patterned channels spatially segregate kinesin motor activity and effectively guide microtubule movements, *Nano Letters*, Vol. 3, No. 5 (2003), pp. 633–637.

(11) Hess, H., Matzke, C.M., Doot, R.K., Clemmens, J., Bachand, G.D., Bunker, B.C., and Vogel, V., Molecular shuttles operating undercover: A new photolithographic approach for the fabrication of structured surfaces supporting directed motility, *Nano Letters*, Vol. 3, No. 12 (2003), pp. 1651–1655.

(12) van den Heuvel, M.G., de Graaff, M.P., and Dekker, C., Molecular sorting by electrical steering of microtubules in kinesin-coated channels, *Science*, Vol. 312, No. 5775 (2006), pp. 910–914.

(13) Sugita, S., *Fundamental study of nano-scale transporting system utilizing kinesin-driven microtubules*, PhD thesis, Tohoku University, 2008.

(14) Zhang, T.Y. and Suen, C.Y., A fast parallel algorithm for thinning digital patterns. *Communications of the ACM*, Vol. 27 (1984), pp. 236–239.

(15) Sugita, S., Sakamoto, N., Ohashi, T., Sato, M., Characterization of motility properties of kinesin-driven microtubules towards nano-scale transporter: focusing on length of microtubules and kinesin density, *Journal of Biomechanical Science and Engineering*, Vol. 3, No. 4 (2008), pp. 510–519.

(16) Kamei, T., Kakuta, S., and Higuchi, H., Biased binding of single molecules and continuous movement of multiple molecules of truncated single-headed kinesin, *Biophysical Journal*, Vol. 88, No. 3 (2005), pp. 2068–2077.

(17) Anderson, C. M., Georgiou, G. N., Morrison, I. E., Stevenson, G. V., and Cherry, R. J., Tracking of cell surface receptors by fluorescence digital imaging microscopy using a charge-coupled device camera. Low-density lipoprotein and influenza virus receptor mobility at 4 degrees C, *Journal of Cell Science*, Vol. 101, (1992), pp. 415–425.

(18) Böhm, K.J., Stracke, R., and Unger, E., Speeding up kinesin-driven microtubule gliding *in vitro* by variation of cofactor composition and physicochemical parameters, *Cell Biology International*, Vol. 24, No. 6 (2000), pp. 335-341.